Environmental Science and Pollution Research (2021) 28:53045–53057
https://doi.org/10.1007/s11356-021-14509-x

RESEARCH ARTICLE

Chromophoric dissolved organic matter (CDOM) in a subtropical estuary (Galveston Bay, USA) and the impact of Hurricane Harvey

Gerardo Gold-Bouchot[1,2] · Samuel Polis[1,2] · Lauren Elizabeth Castañon[1,2,3] · Mayra Padilla Flores[1,2,4] · Alyssa Nicole Alsante[2] · Daniel Conrad Ogilvie Thornton[2]

Received: 19 November 2020 / Accepted: 17 May 2021 / Published online: 22 May 2021

Abstract

The landfall of Hurricane Harvey in August 2017 provided the opportunity to study the impact of extreme freshwater discharge on chromophoric dissolved organic matter (CDOM) properties in a subtropical estuary (Galveston Bay, Texas). Both fluorescence spectroscopy (excitation-emission matrices) and a three-component parallel factor analysis (PARAFAC) model identified changes in CDOM properties. Comparing to Coble's peaks, component 1 was similar to peak C, component 2 to peak M, and component 3 to peak B. Results clearly show three periods with distinct CDOM properties: a dry season, a wet season, and Hurricane Harvey. The dry season was characterized by higher values of the spectral slope and fluorescence and biological indices. The wet season was characterized by high values of PARAFAC components 1 and 2 (humic-like) and the absorption coefficient at 350 nm. Some CDOM components were highly correlated with salinity, indicating conservative mixing. Component 3 (protein-like) had a low correlation to salinity, suggesting degradation or production processes in the bay. Silicates and NO_3^- + NO_2^- had negative relationships with salinity and a positive one with PARAFAC components 1 and 2. PARAFAC component 3 was correlated with dissolved oxygen and chlorophyll *a*, suggesting a relationship between CDOM fluorescent components and phytoplankton activity. High values of the humification index were observed immediately after Hurricane Harvey, indicating increased input of terrestrial organic matter into the bay. Hurricane Harvey increased CDOM levels and humification, and the variability and changes seem to be mostly due to freshwater discharge from the San Jacinto River and not the Trinity River. The influx of freshwater was sufficient to eliminate the salinity gradient in Galveston Bay and significantly change CDOM properties. Galveston Bay recovered quickly from the hurricane and associated flux of freshwater, returning to pre-hurricane CDOM characteristics in less than 2 months.

Keywords PARAFAC · CDOM · EEM · Galveston Bay · Hurricane Harvey · Trinity River · San Jacinto River

Introduction

Hurricane Harvey hit the Texas coast on August 25th, 2017, as a Category 4 hurricane. The storm stalled over Houston for several days, resulting in over 1 meter of rainfall, making it the wettest tropical cyclone recorded in North America (Du et al. 2019; van Oldenborgh et al. 2018). Most of this water ran off into Galveston Bay, which is a highly anthropogenically altered estuary (Al Mukaimi et al. 2018). Estimates of the volume of water discharged into the bay vary; Du et al. (2019) estimated 11.1 × 10^9 m^3 (approximately 3 times the bay's volume) over the following month, whereas Thyng et al. (2020) estimated 22 × 10^9 m^3 (approximately 6 times the bay's volume).

Chromophoric dissolved organic matter (CDOM) is the colored (light-emitting) portion of dissolved organic matter.

Responsible Editor: V. V.S.S. Sarma

✉ Gerardo Gold-Bouchot
ggold@tamu.edu

[1] Geochemical and Environmental Research Group (GERG), College of Geosciences, Texas A&M University, 833 Graham Rd., TX 77845 College Station, USA

[2] Department of Oceanography, College of Geosciences, Texas A&M University, College Station, TX, USA

[3] California State University at Monterey Bay, Monterey County, CA, USA

[4] California State University at Dominguez Hills, Carson, CA, USA

The light emitting properties of CDOM affects water quality, primary productivity, and dissolved oxygen levels (Stedmon et al. 2000). Analysis of CDOM has applications in carbon cycling, tracking of primary productivity, geochemical cycling, and tracing of inputs to water bodies (Kowalczuk et al. 2003). Blough et al. (1993) demonstrated the usefulness of CDOM as a tracer through sampling in the eastern Caribbean Sea. They found areas near the mouth of the Orinoco River had higher concentrations of CDOM than areas further from freshwater sources, indicating that freshwater inputs account for a significant amount of the CDOM in nearby water bodies. CDOM has been used to trace the chemical evolution and transformation of oil in the water column of the Gulf of Mexico following the *Deepwater Horizon* oil spill (Bianchi et al. 2014), and as an indicator of the microbial transformation of organic matter released by phytoplankton (Zheng et al. 2019).

There are few reports of hurricane affects on CDOM dynamics in estuaries. Studies exploring hurricane dynamics have focused on other components of dissolved organic matter (DOM) and have not produced consistent results, possibly due to differences between sites and the storms (i.e., wind speeds, rainfall). Hurricane Irene (2011) resulted in an increase of dissolved organic carbon (DOC) from 7 to 18 mg/L in the Neuse River estuary (Brown et al. 2014), but Hurricane Katrina (2005) produced no significant change in DOC, and only a small, but significant, change in colloidal lignin in the East Pearl river (Shiller et al. 2012). Typhoon Goni resulted in an increase of DOC from 1.2 to 2.48 mgC/L in a mangrove river in Okinawa, Japan (Kida et al. 2018). For Galveston Bay, high CDOM absorption and DOC and low spectral slopes were reported after Harvey (D'Sa et al. 2018), indicating a large input of terrestrial organic matter. In the first week after the storm, floodwaters discharged 87 ± 18 Gg of DOC of terrestrial origin (Yan et al. 2020).

At 1600 km^2, Galveston Bay is the largest estuary in Texas and 7th largest in the USA. Nutrient concentrations are increasing in the bay, resulting in increased eutrophication (Bugica et al. 2020). The main freshwater inputs into the bay are the Trinity and San Jacinto Rivers, with several smaller inputs from bayous. The Trinity River's watershed extends north to the Dallas-Fort Worth metropolitan area and contributes roughly 80% of the freshwater input to the bay. The San Jacinto River's watershed includes the Houston metropolitan area and contributes roughly 10% of the freshwater input to the bay. Together, the two watersheds make a system that is roughly 72,500 km^2 and is home to roughly one half of the state's population. These rivers play an integral role in the water chemistry of Galveston Bay. It has been estimated that 80% of the nitrogen and phosphorus present in the bay are from these two sources. Both rivers are managed, and Lake Houston on the San Jacinto River and Lake Livingston on the Trinity River provide some attenuation of runoff and pollutant loads into the bay (Galveston Bay Estuary Program 2002). Urbanized estuaries, such as Galveston Bay, show changes in the spectroscopic characteristics of CDOM, with increased concentrations of Coble's peak T, a tryptophan-containing protein-like component of CDOM (Tzortziou et al. 2015) associated in particular with sewage discharges in urban environments (Hudson et al. 2007), and decreased aromaticity and relative molecular weight (Gold et al. 2020; Cârstea et al. 2009).

The original objectives of this study were to analyze the spatial and temporal changes of CDOM components in Galveston Bay and to determine if the CDOM components of the two main rivers draining in the bay are different. The landfall of Hurricane Harvey during the study period provided the opportunity to investigate the impact of hurricanes and elevated freshwater discharge on the CDOM components of Galveston Bay. A fire and spill at the Intercontinental Terminal Company (ITC) on the bank of the Houston Ship Channel, in Houston, Texas, on March 2019 (Aly et al. 2020) was an additional event with the potential to affect CDOM components in Galveston Bay during the study period.

We hypothesize that terrestrial CDOM components increased after Hurricane Harvey, they are different in the dry months from those in the rainy months, and that CDOM has a more urbanized signature in the San Jacinto River than in the Trinity River due to differences in their catchment areas.

Methods

Water samples were taken at eight stations in a sampling design from the mouth of the Trinity River (the main source of freshwater into the bay) to the main opening into the Gulf of Mexico (Fig. 1). Samples were taken at six sampling stations using 5 L Niskin bottles, at the surface (1 m depth) and bottom (1 m above the bottom) of Galveston Bay, Texas (Fig. 1), during June and September, and in nine sampling stations in November of 2017; March, June, September, and November 2018; and March 2019. In March 2019, additional samples were taken as close as possible to the chemical spill site from the ITC facilities (Aly et al. 2020). In June 2019, samples were collected in triplicate from both the Trinity and San Jacinto Rivers (Fig. 1) to evaluate the two main sources of freshwater into Galveston Bay.

Salinity was measured from water samples taken from the Niskin bottles and measured in a GuildLine Instruments Model 8400B salinometer. Salinity was calculated from conductivity using the equation for practical salinity by UNESCO/ICES/SCOR/IAPSO (1980). Nutrients were analyzed using an Astoria-Pacific Analyzer. Nitrates and nitrites were analyzed following the method by Armstrong et al. (1967), ammonium by the method of Harwood and Kuhn (1970), silicates by the method of Armstrong et al. (1967),

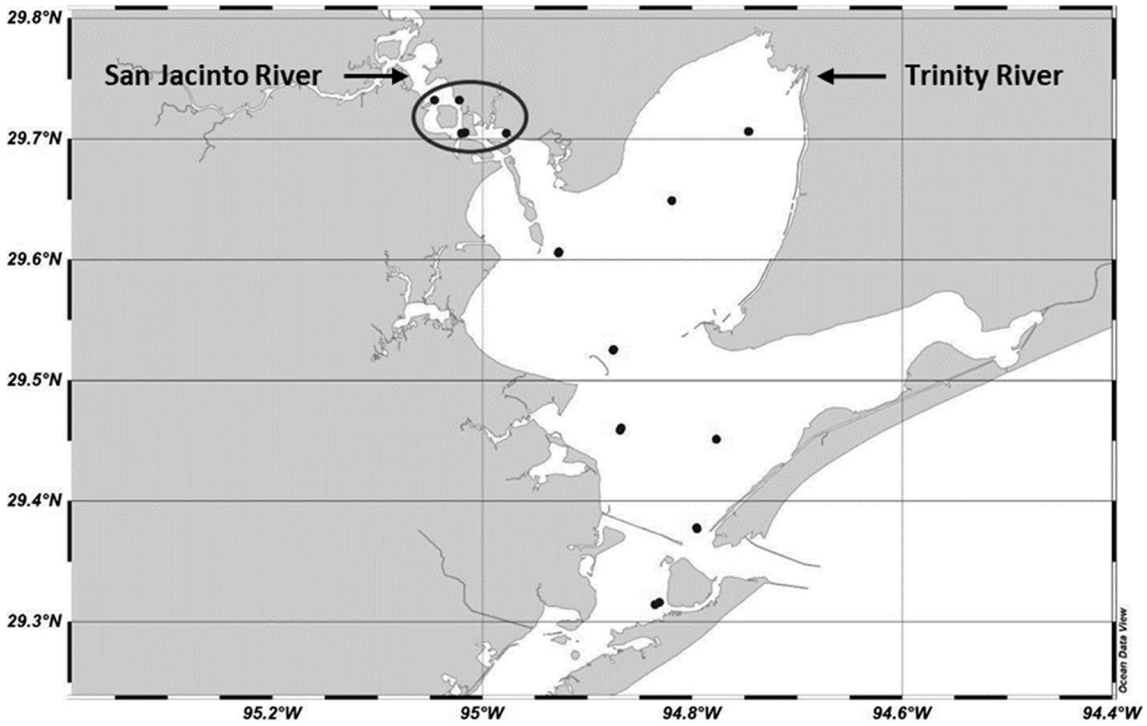

Fig. 1 Galveston Bay, with the sampling stations used in this study. Stations circled were added in March 2019 close to the Intercontinental Terminals Company (ITC) facilities and are close to the mouth of the San Jacinto River

and orthophosphates by the method of Bernhardt and Wilhelms (1967). Dissolved oxygen was determined by the Winkler titration method (Strickland and Parsons 1972) using a potentiometric titrator. Dissolved oxygen data is not available for the September 2017 sample collection.

Water samples from the Niskin bottles were filtered onto 47-mm glass fiber filters (GF/C, Whatman) for pigment analysis. The filters were placed in 15 mL centrifuge tubes kept on dry ice in the dark and transferred to a − 20 °C freezer on return to the laboratory. Chlorophyll *a* was extracted from the filters using 10 mL of ice-cold 90% acetone in centrifuge tubes. Following sonication (QSonica Q125) for 1 min, the filters were extracted overnight at 4 °C in the dark. The following day, the pigment extraction was centrifuged to remove suspended particles, and the supernatant was decanted and diluted 10-fold if the extraction was visibly green. For analysis, 3 mL aliquots were placed in quartz glass cuvettes (10 mm, Firefly Sci.), and chlorophyll *a* concentration was measured by fluorescence using a TD-700 fluorometer (Turner Designs) calibrated with a chlorophyll *a* standard (Arar and Collins 1997).

For CDOM absorbance and fluorescence, water samples were gravity-filtered through pre-combusted glass fiber filters (GF/C, Whatman). Excitation-emission matrices (EEM) and absorbance spectra were obtained with a Horiba Aqualog fluorometer in a 1-cm quartz cuvette, with excitation wavelengths from 240 to 500 nm every 2 nm. Emission values were recorded every 2 nm. Fluorescence and absorption spectra were corrected by subtracting a high-purity water sample (Raman Water Fluorescence Reference, Starna Scientific). Following the procedure of Kothawala et al. (2013), fluorescence spectra were corrected by inner filter effect using the Aqualog software, and intensities were converted to Raman units (excitation at 350 nm, emission from 371 to 428 nm) (Lawaetz and Stedmon 2009) using the daily high-purity standard. Fluorescence (intensity at 450 nm divided by the intensity at 500 nm, both at 370 nm excitation (McKnight et al. 2001)), humification (ratio of the sum of the fluorescence between 435 and 480 nm and between 300 and 345 nm at a fixed excitation of 254 nm (Ohno 2002)), and biological or freshness (intensity 380 nm divided by the intensity at 430 nm, both at an excitation of 310 nm (Huguet et al. 2009)) indices were calculated (Gabor et al. 2014) using the "eemR" package (Massicotte and Markager 2016).

Absorbance measurements were converted to Napierian absorption coefficients by:

$$a(\lambda) = 2.303\ \mathrm{A}(\lambda)/l$$

where $a(\lambda)$ is the absorption coefficient at wavelength λ, A(λ) is the measured absorbance at wavelength λ, and l is the cuvette path length in meters. The absorption coefficient at 350 nm (a_{350}) was used as a proxy for CDOM concentrations (Massicotte et al. 2017). Spectral slopes (S) of absorption spectra (Loiselle et al. 2009) were calculated by fitting a Gaussian curve to the spectra in the 240 to 500 nm range. Spectral slope ratios (Sr) (Helms et al. 2008) were calculated

as the ratio of the slope from 275 to 295 nm divided by the slope from 350 to 400 nm. Spectral slopes and spectral slope ratios were calculated using the "cdom" package (Massicotte and Markager 2016). Packages "eemR" and "cdom" were run with R version 3.5.2 (R Core Team 2018).

A parallel factor analysis (PARAFAC) model was fitted to the fluorescence data (Stedmon et al. 2003) using the "drEEM" toolbox version 0.5 for MATLAB (MathWorks Inc.) (Murphy et al. 2013). A model was fitted to the data using non-negativity constraints in all modes. During the exploratory phase, one sample and one excitation wavelength were removed due to high leverage, leaving a total of 122 samples in the dataset. The intensities of fluorescence of the four components are reported relative to the maximum intensity of each component. A three-component model was fitted to the data, with a core consistency of 74.3 and a fit of 96.6%. The model was validated using split-half analysis (Stedmon and Bro 2008).

A permutational multivariate analysis of variance (Anderson 2001) was performed on the PARAFAC components, the three fluorescence indices, a_{350}, S, and Sr by transforming the data using the Hellinger transformation (Legendre and Gallagher 2001) with the Euclidean dissimilarity index with 9999 permutations. Function "nested.anova.dbrda" in package "BiodiversityR" was used. A *post hoc* test was performed with the function "betadisper" in package "vegan," correcting by bias (Stier et al. 2013). Both packages were used with *R* version 3.5.2. Redundancy Analysis (RDA) was done using CANOCO (version 5.12) (ter Brak and Šmilauer 2012). Maps were made with Ocean Data View version 5.2.1 (Schlitzer 2020. Ocean Data View. https://odv.awi.de).

Results and discussion

Spectral loadings and excitation-emission plots for the three components of the PARAFAC model are shown in Fig. 2. Component 1 has an excitation wavelength of 336 nm and emission at 489 nm; component 2 has an excitation wavelength of 292 nm and emission at 394 nm; and component 3 has excitation at 280 nm and emission at 317 nm. Component 1 is similar to peak C, component 2 to peak M, and component 3 to peak B (Stedmon et al. 2003; Coble 1996, 2007). Results were incorporated into the OpenFluor online database (Murphy et al. 2014) and compared with other results with a similarity of 0.95 or higher. Components 1, 2, and 3 are similar to components D, B, and C, respectively, in Shutova et al. (2014), who interpreted their component D as peaks A and C, component B as humic-like, and component C as protein-like. Component 1 is component 1 in Catalá et al. (2015), Tanaka et al. (2014), and Kulkarni et al. (2018) who all interpreted it as a humic-like component. Component 2 is component 2 in Kulkarni et al. (2018) who interpreted it as a humic-like component, and component 3 is component 5 in Yamashita et al. (2010) who interpreted it as a protein-like component.

There were no significant differences between the surface and bottom samples (t-test, all P values above 0.05) for all parameters analyzed, and all values were combined for further analysis. In September 2017, immediately after Harvey made landfall in the Houston area, none of the parameters had a significant correlation with salinity, likely due to the very large amount of water going through the bay (D'Sa et al. 2018) eliminating the salinity gradient from the Trinity and San Jacinto Rivers. Salinity in September 2017 dropped from a median value of approximately 16 ppt in June 2017 to 3.4 ppt and increased to 16 ppt again in November 2017. The highest median salinity values were observed in June 2018, with a median value of 25.9 ppt (Fig. 3).

The minimum median temperature (17.3 °C) was observed in March 2019 and the maximum (30.2 °C) in June 2018, which was also the driest month (Fig. 3A). The minimum median dissolved oxygen concentration (171 μmol/L) was observed in June 2018 when salinity was highest. The lowest temperature (Fig. 3C) was associated with the highest median oxygen concentration (360 μmol/L) in March 2019. The lowest median chlorophyll *a* concentration (5.6 μg/L) was

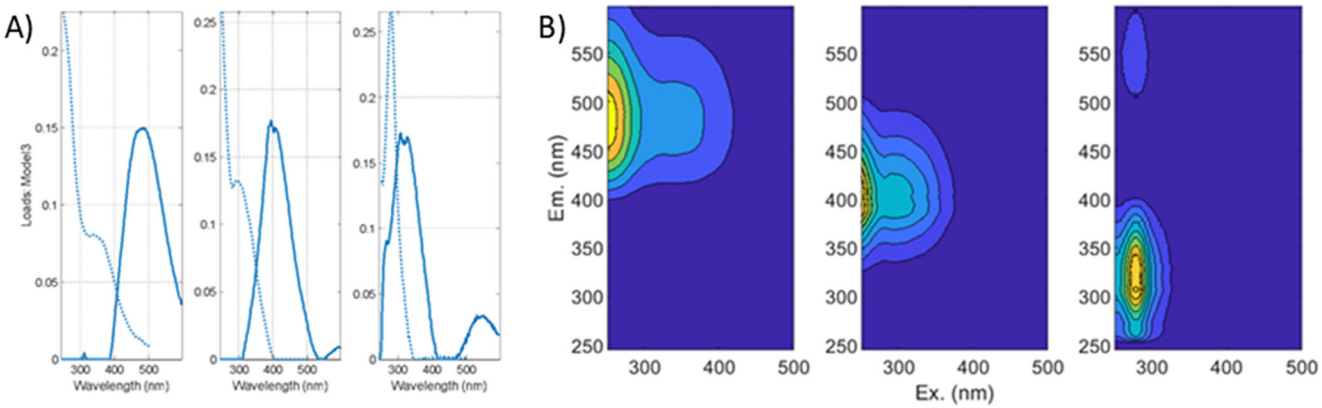

Fig. 2 Spectral loadings (**A**) and excitation-emission plots (**B**) for the three components of the PARAFAC model obtained for Galveston Bay, color-coded for fluorescence intensity in Raman units

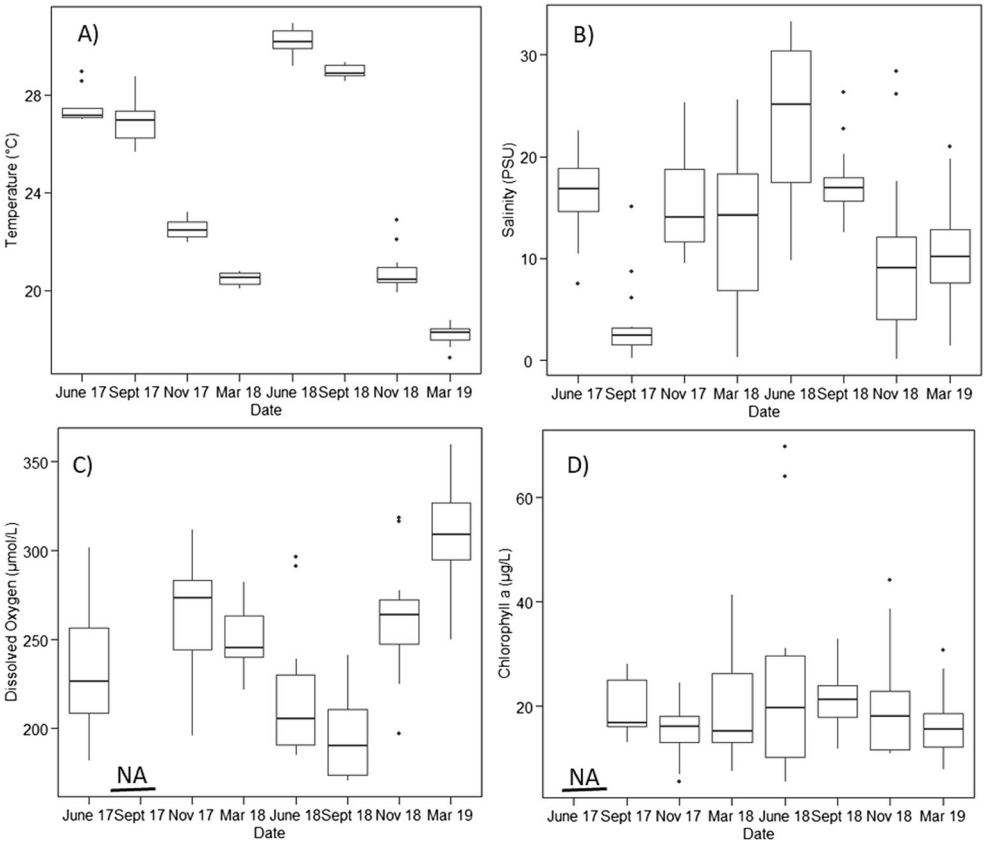

Fig. 3 Boxplot of the median (± interquartile range, IQR; whiskers are ± 1.5*IQR) of **A** temperature, **B** salinity, **C** dissolved oxygen, and **D** chlorophyll *a* values in Galveston Bay. NA = not available

observed in November 2017, whereas the highest (21.2 µg/L) was in June 2018 (Fig. 3D). June 2018 had the highest median salinities, temperatures, and chlorophyll *a* values.

Relatively high and variable nitrate plus nitrite (NO_3^- + NO_2^-) concentrations were observed in Galveston Bay during the last two surveys (November 2018 and March 2019), whereas nitrate plus nitrite concentrations were low and relatively constant on all other sampling occasions (Fig. 4). Ammonium and phosphates had a similar temporal pattern, with maximum median values in November 2017 (Fig. 4). Silicates had a significant inverse relationship with salinity, suggesting conservative mixing. There were some outlying values corresponding to the March 2019 sampling (Fig. 1, Supplementary Information). The spatial distribution of salinity follows a distinct pattern, increasing to the south as sampling stations get closer to the mouth of the estuary (Fig. 5). The gradient was stronger during the driest month (June 2018), and there was no salinity gradient a few days after Hurricane Harvey (September 2017).

The humification index (HIX) and spectral slope (S) did not show a strong spatial gradient, except for HIX in the September 2017 sampling, with values increasing to the south (Fig. 5), suggesting more recalcitrant organic matter in the bay. HIX also showed a large increase after Hurricane Harvey (Fig. 6A), indicating an increase of humification and relative molecular weight, consistent with the results of humic-like PARAFAC components 1 and 2 (Fig. 7A and B).

PARAFAC components 1 and 2 show a significant increase in after Hurricane Harvey (September 2017), indicating a large input of terrestrial organic matter into the bay (Fig. 7A and B). PARAFAC component 3 does not show an increase after Hurricane Harvey but relatively low values for the first sampling months, and then a slow increase later on (Fig. 7C). PARAFAC components 1 and 2 had different spatial distributions, with maximum and minimum values in different places and input from the Trinity and San Jacinto Rivers and evidence of production mid-bay. Component 3 had a different spatial pattern than both components 1 and 2, with clearer input from the two rivers draining into the bay (Fig. 8).

The biological or freshness index had a decrease during September 2017 when Hurricane Harvey hit (Fig. 6B). The spectral slope had a slight decrease in September 2017 to 0.013 nm^{-1}, but for all the other months, the values were in the range from 0.014 to 0.016 nm^{-1} (Fig. 6C). The spectral slope ratio had a temporal behavior similar to that of the protein-like PARAFAC component 3, with values increasing from June 2017 to maximum values in June and September 2018 and decreasing slightly in November 2018 and March 2019 (Fig. 6D). The fluorescence index did not show any temporal trends, with monthly means between 1.2 and

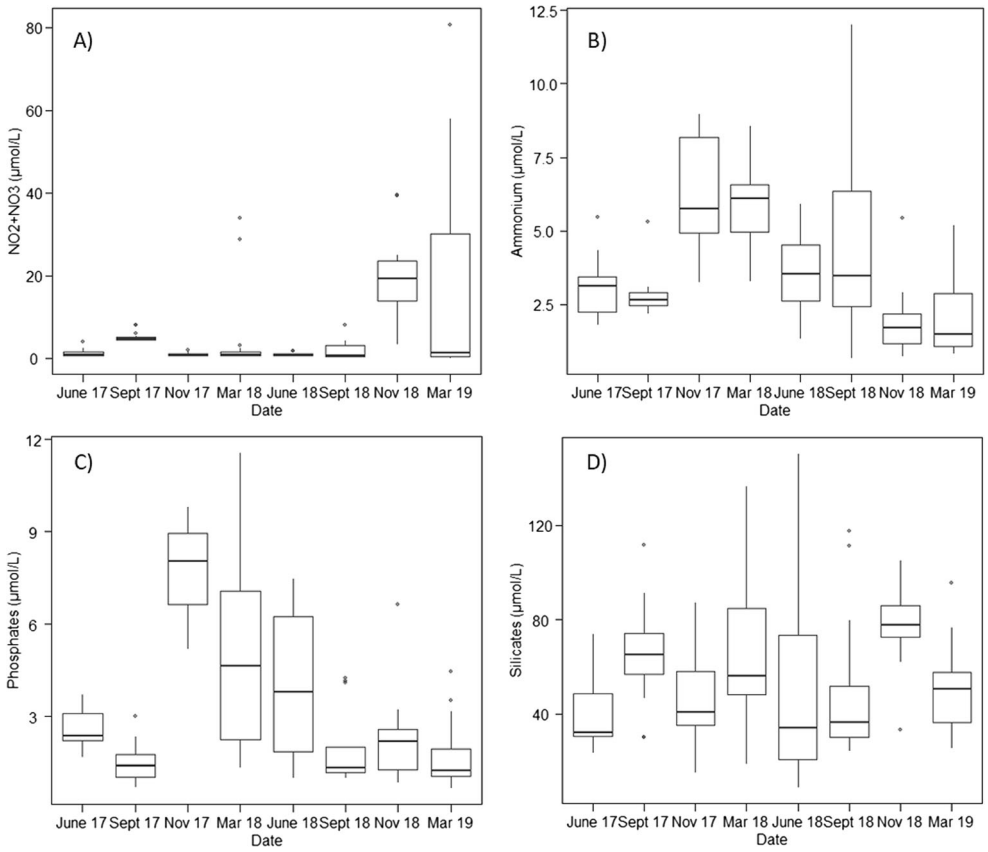

Fig. 4 Boxplot of the median (± interquartile range, IQR; whiskers are ± 1.5*IQR) of **A** nitrates plus nitrites, **B** ammonium, **C** phosphates, and **D** silicate concentrations in Galveston Bay

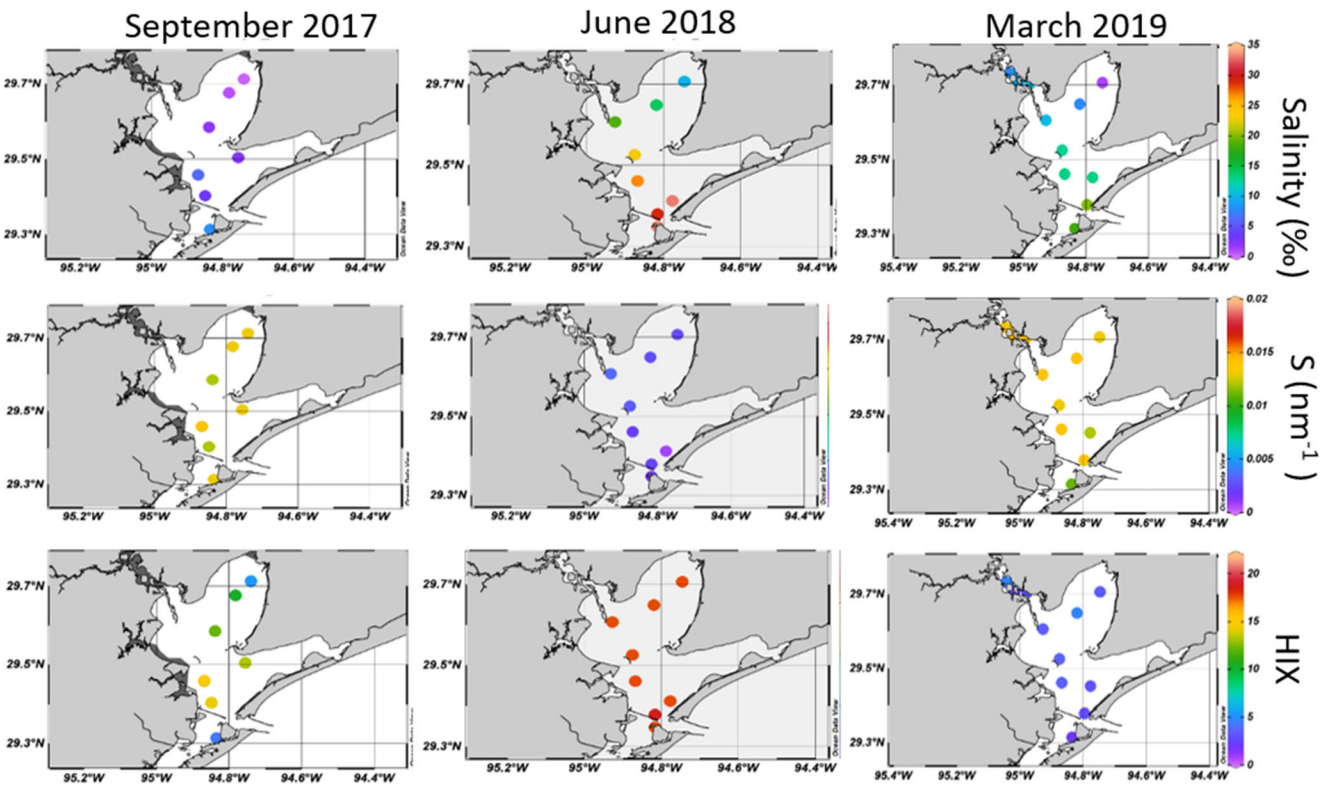

Fig. 5 Spatial distribution of salinity, spectral slope (S), and the humification index (HIX) in Galveston Bay during September 2017 (Hurricane Harvey), June 2018 (highest salinity), and March 2019

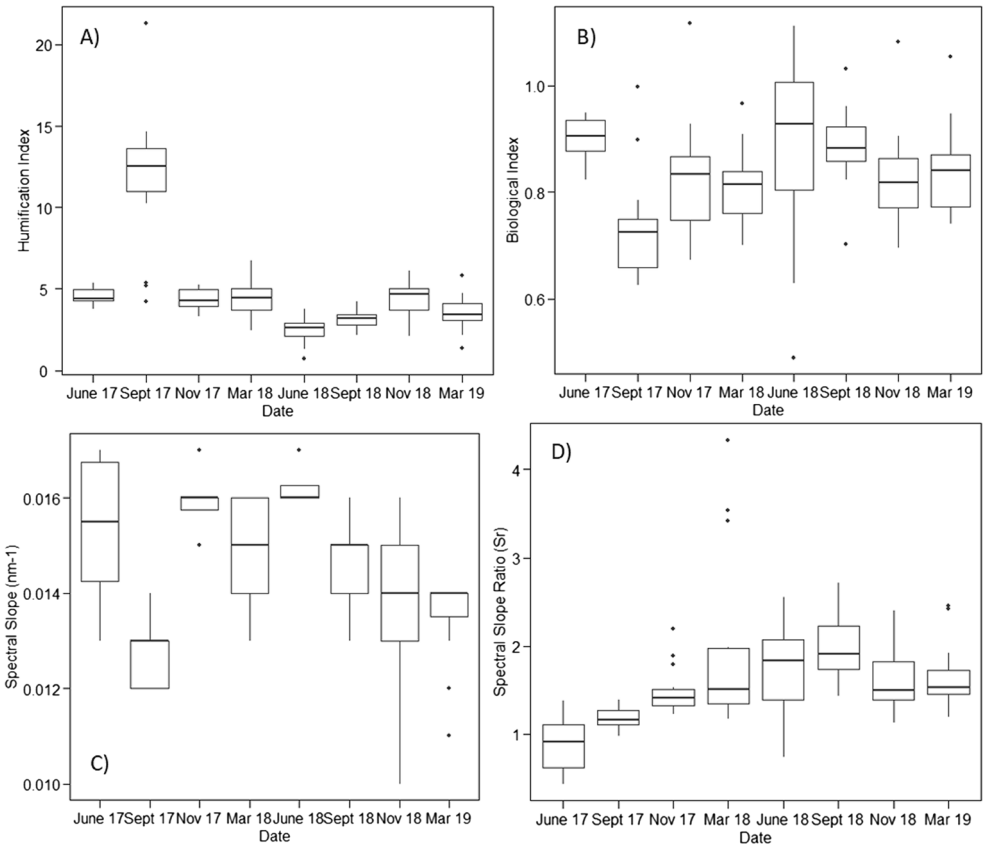

Fig. 6 Boxplots of the median (± interquartile range,IQR; whiskers are ± 1.5*IQR) of humification index (**A**), biological (or freshness) index (**B**), spectral slope (S) (**C**), and spectral slope ratio (SR) (**D**) values per sampling cruise in Galveston Bay

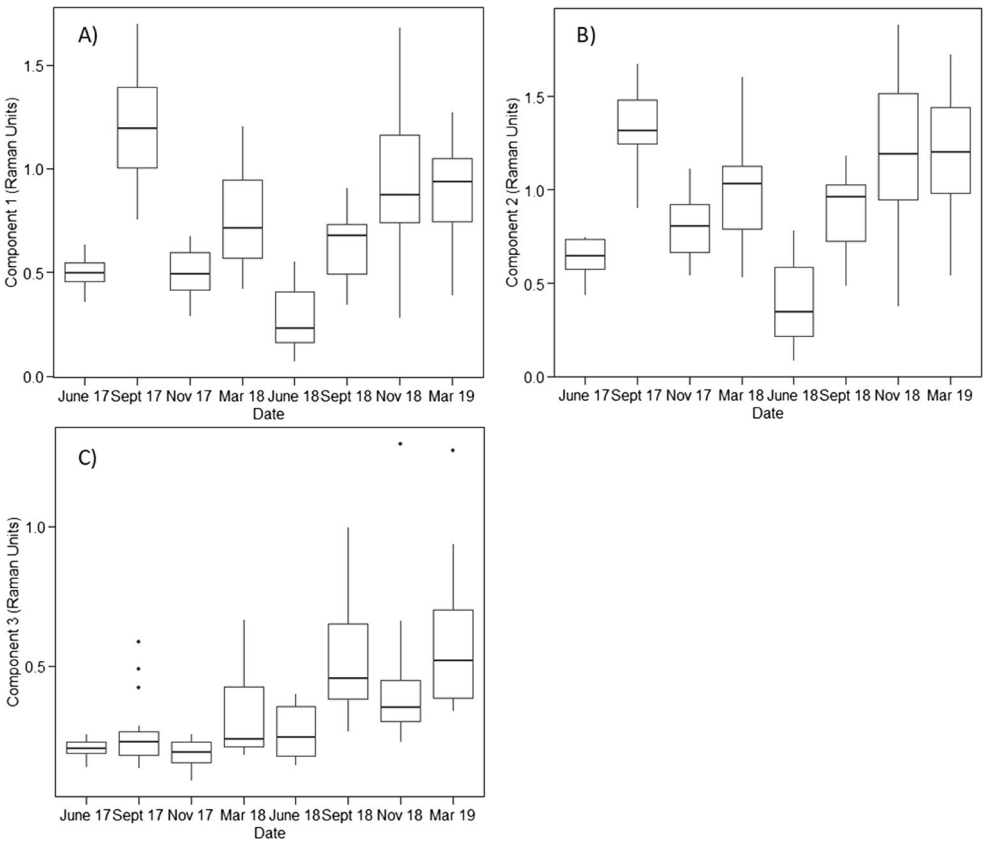

Fig. 7 Boxplots of the median (± interquartile range, IQR; whiskers are ± 1.5*IQR) of PARAFAC component 1 (**A**), PARAFAC component 2 (**B**), and PARAFAC component 3 (**C**) values in Galveston Bay. Values for all components are in Raman units

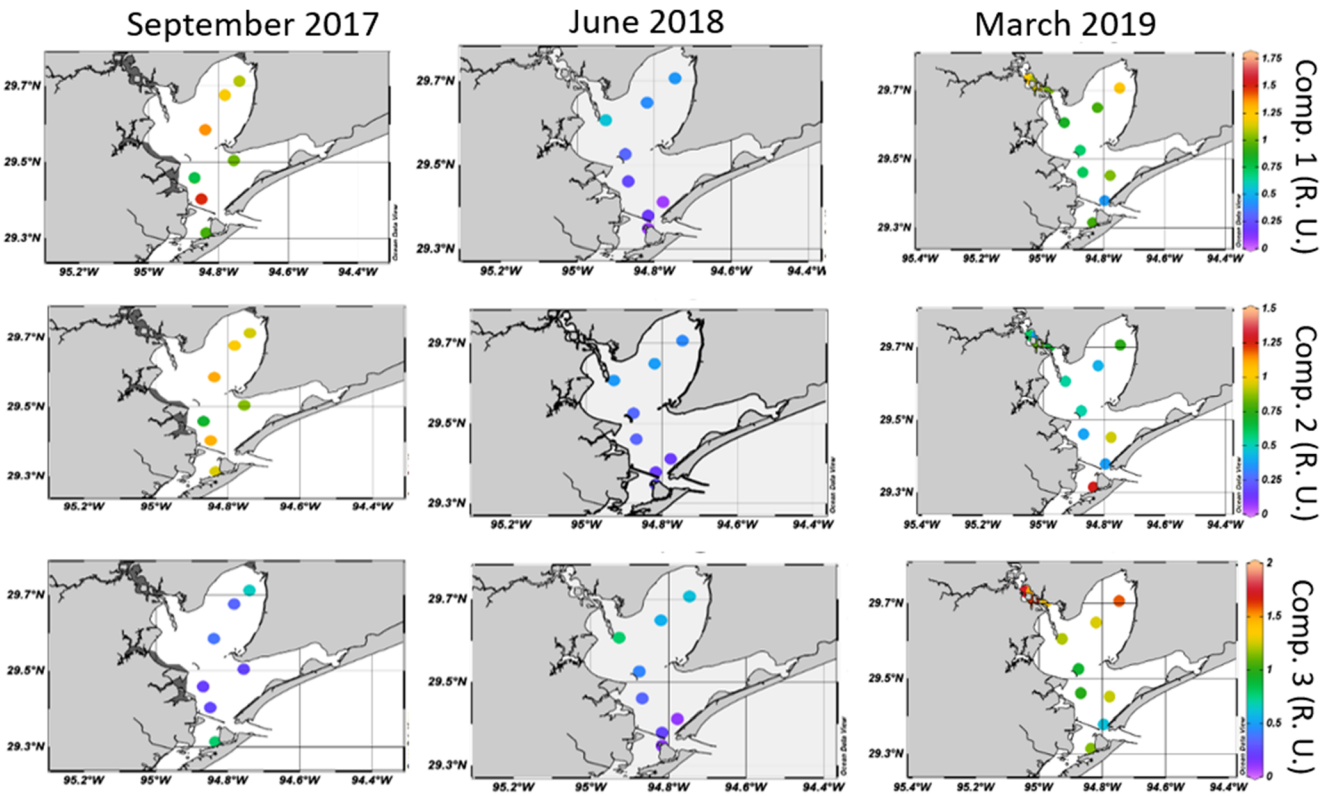

Fig. 8 Spatial distribution of the three PARAFAC components in Galveston Bay during September 2017, June 2018, and March 2019

1.3, suggesting that the dissolved organic matter in the bay is mostly of terrestrial origin (Fig. 2, Supplementary Material).

The absorption coefficient at 350 nm (a_{350}), which is correlated with total CDOM concentration, showed an increase in September 2017, after Hurricane Harvey, from 3.05 m^{-1} in June 2017 to 13.8 m^{-1} in September 2017, the highest median value for all the samplings (Fig. 3, Supplementary Material).

PARAFAC components 1 and 2 show a negative relationship with salinity, indicating conservative mixing, with the main input from the Trinity River except after Hurricane Harvey when our results suggest a higher input from the San Jacinto River. PARAFAC component 3 did not show a conservative mixing behavior, with possible sources in the bay (Fig. 4, Supplementary Information. The relationship of component 2 with salinity is identical to that of Component 1, and it is not shown). Galveston Bay is increasingly eutrophic (Bugica et al. 2020), and increased primary productivity could explain the non-conservative behavior of component 3.

The humification index shows an interesting behavior with respect to salinity (Fig. 5, Supplementary Material), with September 2017 (shown in the box in Fig. 5 in the Supplementary Information) sampling clearly separated from all the other months. If the September 2017 data associated with Hurricane Harvey were omitted from the analysis, then there was a tendency for the humidification index to decrease towards higher salinities, consistent with lower humification and lower molecular weight CDOM in seawater. Similar behavior was reported for the Evros river in the Balkans (Tzortziou et al. 2015).

The spectral slope had a slight decrease in September 2017 to 0.013 nm^{-1}, but for all the other months, the values were in the range of 0.010 to 0.017 nm^{-1} (Fig. 6C). The fluorescence index did not show any temporal trends, with monthly means between 1.2 and 1.3, suggesting DOM in the bay is mostly of terrestrial origin (Fig. 1, Supplementary Material).

The results for the September 2017 samples, taken a few days after Hurricane Harvey, were statistically different from the other months. Taking all results, a permutation nested (sampling stations nested in month) MANOVA was highly significant (Table 1):

Over the course of this study, there was high environmental variability, with a very wet September 2017 (lowest median salinities, Fig. 3) due to Hurricane Harvey and a dry June 2018 month (highest median salinity, Fig. 3). Using principal component analysis with normalized values for all sampling trips

Table 1 Permutation-based nested MANOVA using 9,999 permutations

	df	Sum of Squares	F	Pr(>F)
Date	7	0.049151	8.9389	0.0001
Station	36	0.028278	3.8775	0.0001
Residual	70	0.014181		

(Fig. 9), the first axis explains 41.3% of total variance, and the second axis explains 27% of total variance, for a total explained variance for the first two axes of 68.3%.

The highest loadings (in absolute value) for the PCA first axis are PARAFAC components 1 and 2, spectral slope, biological index, and salinity. For the second axis, the highest absolute loadings are PARAFAC component 3, spectral slope ratio, and the humification index. Lower salinities, associated with more rainfall, increase variability due to increased freshwater inputs to the bay with increased sources of CDOM. The increase in CDOM can be explained by high discharge from the Trinity and San Jacinto Rivers in the wet months. Additionally, the surrounding land area around the bay contains highly urbanized (City of Houston, Texas) and agricultural areas. Surface runoff into the bay during wet periods could also increase the variability of CDOM present.

A redundancy analysis using salinity, nutrients, chlorophyll *a* and month as independent variables, and dry and wet seasons as supplementary analysis, explained 45.1% of total variance (Šmilauer and Lepš 2014) as shown in Fig. 10.

The first axis that accounts for 31.3% of the total variance is negatively related to salinity and the fluorescence and biological indices; it is positively related to PARAFAC components 1 and 2, silicates and $NO_3^- + NO_2^-$. The second axis that accounts for 7.75% of total variance is negatively related to PARAFAC component 3, dissolved oxygen, and chlorophyll *a*. Axis 1 separates the wet months, March, September, and November 2018 and March 2019, from the dry months. Axis 2 divides September 2017 (Hurricane Harvey) from the other months.

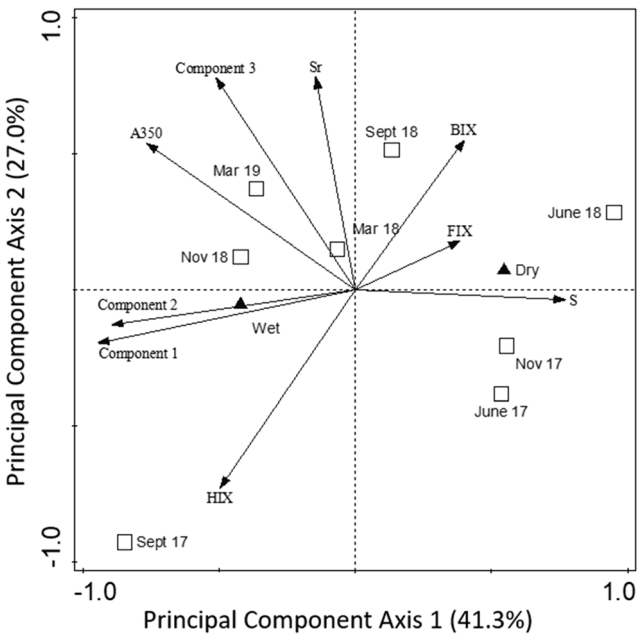

Fig. 9 Principal component analysis of CDOM results for Galveston Bay. Total variance explained by the first two axes is 68.6%. S = spectral slope, FIX = fluorescence index, BIX = biological index, A350 = absorption coefficient at 350 nm, SR = spectral slope ratio, HIX = humification index

CDOM results are different for the Trinity and San Jacinto Rivers as they enter Galveston Bay (Fig. 10), with humic-like and protein-like components and *a*350 higher in the San Jacinto than in the Trinity River. The spectral slope ratio is higher in the Trinity than in the San Jacinto. These spectroscopic characteristics agree with the signature of urbanized estuaries (Gold et al. 2020). Changing rainfall patterns may influence the relative proportions of San Jacinto and Trinity River water entering the bay and thus changing the spectral signature of CDOM in the bay.

A permutation multivariate nested ANOVA test showed a highly significant effect by month (Table 1). A redundancy analysis (RDA), the constrained form of principal component analysis, clearly shows the September 2017 sampling completely separated from the other months (Fig. 10). After Hurricane Harvey, there was a significant input of terrestrial organic matter (a 4.5-fold increase from June to September 2017, as indicated by a_{350}), with a terrestrial signature as determined by an increase in PARAFAC components 1 and 2, and the humification index. A decreased biological (or freshness) index indicates older, more degraded CDOM. The only significant positive correlation with salinity was the fluorescence index in November, with a significantly higher slope at the bottom. It went from values around 1.2 in the upper bay with salinities of 9 PSU, indicating a terrestrial origin, to values around 1.8 in the lower bay with salinities of 25 PSU, indicating a microbial origin (Gabor et al. 2014). These results suggest that as the water flows down the bay, processes other than conservative mixing are contributing to these patterns, such as microbial degradation or CDOM input from marshes and other vegetation around the bay (Catalá et al. 2013). A small but significant decrease in spectral slope indicates the new organic matter has a higher average molecular weight than before or after the storm.

After the September 2017 sampling when Hurricane Harvey hit, PARAFAC components 1 and 2, *a*350, and HIX values went back to their previous values by the November 2017 sampling, with a clear difference between the September versus the June and November results (Figs. 6 and 7). Water properties measured in June and November 2017 were not significantly different, indicating rapid recovery from the elevated flux of freshwater into Galveston Bay caused by Hurricane Harvey in August 2017. This is consistent with a two-month recovery period for Galveston Bay after Hurricane Harvey reported by D'Sa et al. (2018), Liu et al. (2019), and Du et al. (2019), indicating a high resiliency for this ecosystem.

The variability of CDOM components increases with decreasing salinity, associated with increased rainfall (Fig. 10). More rainfall can produce flooding of areas adjacent to the riverbanks or areas usually not flooded, and this can contribute other sources of CDOM, such as riparian vegetation as reported for Mediterranean rivers (Catalá et al. 2013). PARAFAC

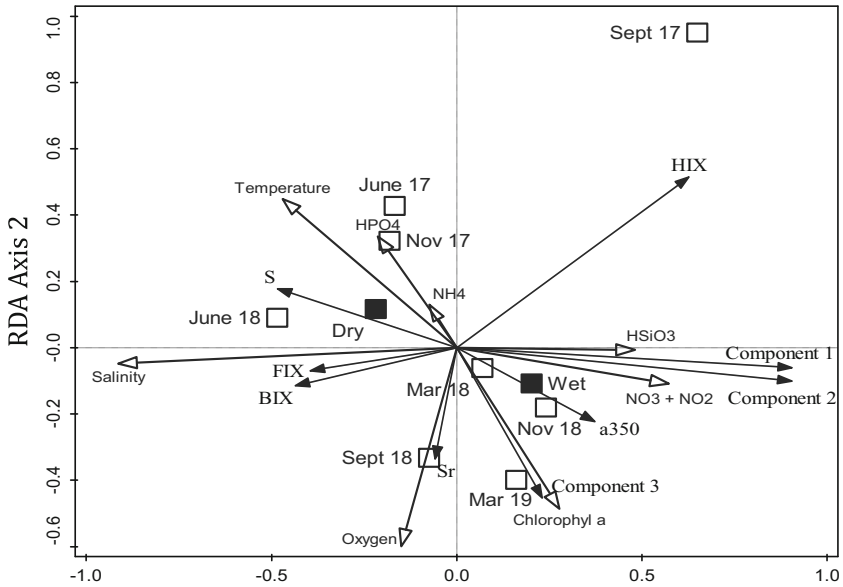

Fig. 10 Redundancy analysis (RDA) of CDOM results for Galveston Bay. Months are represented by open squares and quantitative variables as open arrows. Dry and wet seasons were used as supplementary variables and are shown as filled triangles. Sampling stations are not shown for clarity. Explanatory variables account for 45.1% of the total variance. Permutation test (9999 permutations) for all axes: pseudo-F = 9.5, P = 0.0001

components 1 and 2 and the humification index have high positive loadings for the first PCA axis, while salinity has a high negative loading (Table 1, Supplementary Material). This agrees with the interpretation given to these components and HIX, as representing humic terrestrial CDOM. Lu and Liu (2019) observed an increase in lignin, tannin, and condensed aromatic compounds during high flow conditions in south Texas rivers, which agrees with our observations in Galveston Bay after Harvey. PARAFAC component 3, which is a protein-like component, and the spectral slope ratio have high loadings for axis 2 (Table 1, Supplementary Material). PARAFAC component 3 and the spectral slope ratio do not have conservative mixing,

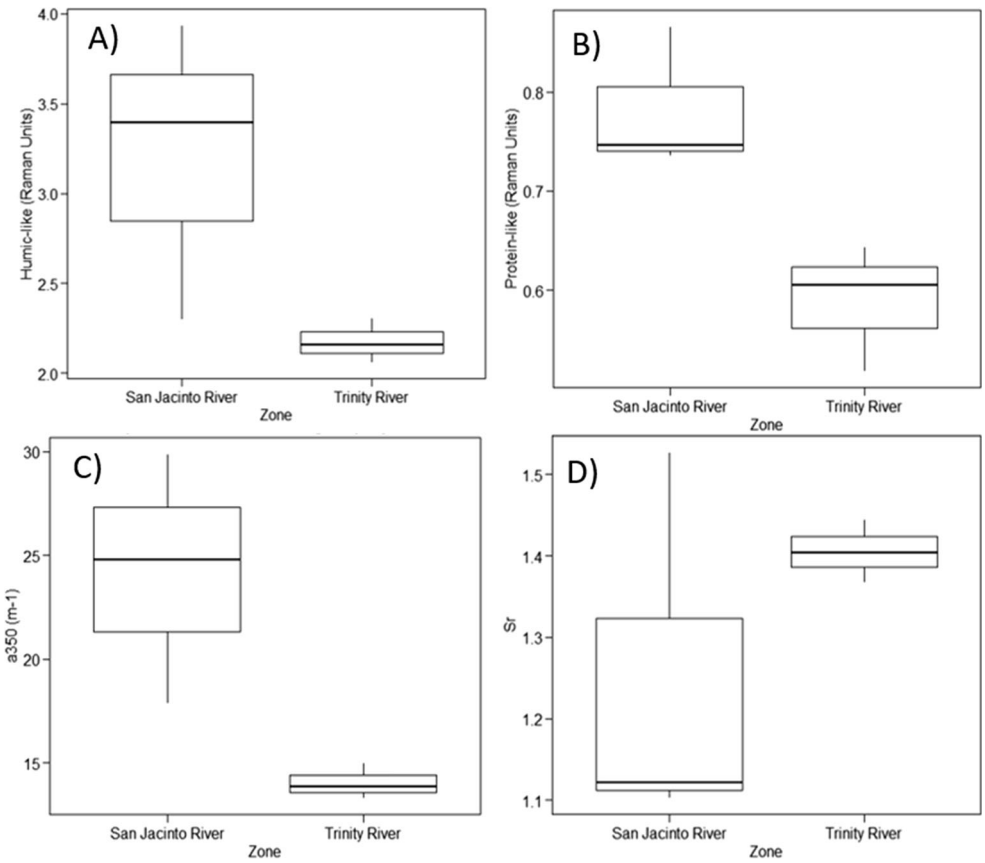

Fig. 11 Boxplots of median (± interquartile range) values of protein-like (in Raman units) (**A**), humic-like (in Raman units) (**B**), absorption coefficient at 350 nm (a_{350}) (in m^{-1}) (**C**), and spectral slope (SR) (in nm^{-1}) (**D**) from the Trinity and San Jacinto Rivers in March 2019

shown as a not significant relation with salinity (Fig. 4, Supplementary Material), and both show an increase at medium salinities (15-20 PSU), suggesting increased biological activity in the estuary. Yan et al. (2020) reported a similar effect when analyzing the distribution of DOC. PARAFAC components 1 and 2 had a significant relationship with silicates, as shown by the small angle between the arrows of both PARAFAC components and that of silicates (Fig. 10) and linear relationships between both components and silicates (Fig. 6, Supplementary Material), suggesting a relationship with phytoplankton activity. At low NO_3^- + NO_2^- concentrations, component 2 increases and then remains constant (Fig. 6). The relationship of PARAFAC components 1 and 2 with silicates and NO_3^- + NO_2^- could also indicate a relationship with primary productivity in the bay (Fig. 10), but the relationship with chlorophyll is not strog.

Based on samples collected in the mouth of the Trinity River in March 2019 (Fig. 11), the source of increased humification was likely the San Jacinto River, rather than the Trinity River. This could be due to differences in their catchment areas. The San Jacinto River flows into Galveston Bay through a highly urbanized and industrialized area in the Houston metropolitan area, whereas the Trinity River is much longer and goes mainly through agricultural and forest areas before draining into Galveston Bay. Higher values of protein-like peaks (particularly peak T) in the San Jacinto River agree with the spectroscopic signal of urbanized rivers, mostly from sewage discharges (Cârstea et al. 2009; Hudson et al. 2007; Tzortziou et al. 2015). The CDOM pattern observed after hurricane Harvey in the September 2017 sampling (i.e., increased humic-like and protein-like components) and absorption coefficient at 350 nm (a_{350}) and decreased spectral slope (Figs. 6 and 7) resembles the differences between the Trinity and San Jacinto Rivers (Fig. 11). This suggests changes observed in the September 2017 sampling (right after Harvey) were due mostly from discharges from the San Jacinto River rather than from the Trinity River, agreeing with results from D'Sa et al. (2018), Yan et al. (2020), Steichen et al. (2020), and Valle-Levison et al. (2020). This is supported by the fact that during the first few weeks after Harvey, the main flow of freshwater into the bay was the San Jacinto River (approximately 3300 m^3/s) and not the Trinity River (approximately 2500 m^3/s) (D'Sa et al. 2018; Liu et al. 2019; Yan et al. 2020). Warnken and Santschi (2004) observed a linear increase of DOC into the bay with an increasing flow from the Trinity River, but during tropical storm Allison the Trinity River had reduced DOC concentrations.

Conclusions

High environmental variability driven by salinity changes reflected in CDOM components was observed over a 2-year period in Galveston Bay. Higher CDOM variability was associated with lower salinities during high precipitation seasons. Both silicates and NO_3^- + NO_2^- had a negative relationship with salinity and a positive relationship with PARAFAC components 1 and 2, while PARAFAC component 3 had a positive relationship with dissolved oxygen and chlorophyll *a*. These results suggest a relationship of CDOM fluorescent components and phytoplankton activity in the bay. Three distinct groups of results are observed: the wet and dry seasons and Hurricane Harvey. In particular, June 2018 stood out with the highest median salinity, temperature, and chlorophyll *a* values. Important differences were observed between the CDOM signatures of the San Jacinto and Trinity Rivers, with a more urbanized signal from the San Jacinto River. There was a significant impact by Hurricane Harvey on CDOM components in Galveston Bay, particularly an increase in the humification index, mostly due to the discharge of the San Jacinto River and not to the Trinity River, which is usually the main source of freshwater into the bay.

Supplementary Information The online version contains supplementary material available at https://doi.org/10.1007/s11356-021-14509-x.

Acknowledgments We thank the two anonymous reviewers for their helpful suggestions. The authors thank the crew of the R/V Trident, and all the participants in the cruises for their help during the fieldwork and Dr. Piers Chapman for salinity analysis and Kusumica Mitra for nutrient analysis (GERG).

Availability of data and materials The datasets used and/or analyzed during the current study are freely available at the Texas Data Repository at: https://urldefense.com/v3/__https://dataverse.tdl.org/dataset.xhtml?persistentId=doi:10.18738*T8*EMSIOL__;Ly8!!KwNVnqRv!QqPkRXx0xcKybrAKdhn1NDUYUqnK-rw_ijLjpVBOOKcbiIQ2Gvw7daGHbFEnzA$

Author contribution GGB designed the study, helped analyze the samples, did data and PARAFAC analysis, and helped write the manuscript. ANA participated in the fieldwork, analyzed samples, and helped write the manuscript. DCOT helped design the study and contributed to the manuscript. SP participated in fieldwork, analyzed samples, helped do the PARAFAC and data analyses, and helped write the manuscript. LC and MP participated in the fieldwork, helped analyze the samples, and helped write the manuscript.

Funding This work was partially funded by a Texas A&M University "T3 Triads for Success" grant. LC, MP, and SP thank a fellowship from the NSF Research Experience for Undergraduates (REU) "Observing the Ocean" program at the Oceanography Department, Texas A&M University (grants OCE-1455851 and OCE-1849932).

Declarations

Ethics approval and consent to participate Not applicable

Consent for publication Not applicable

Competing Interests The authors declare that they have no competing interests.

References

Al Mukaimi ME, Kaiser K, Williams JR, Dellapenna TM, Louchouarn P, Santschi P (2018) Centennial record of anthropogenic impacts in Galveston Bay: evidence from trace metals (Hg, Pb, Ni, Zn) and lignin oxidation products. Environ Pollut 237:887–899. https://doi.org/10.1016/j.envpol.2018.01.027

Aly NA, Luo Y-S, Liu Y, Casillas G, McDonald TJ, Kaihatu JM, Jun M, Ellis M, Gossett S, Dodds JN, Baker ES, Bhandari S, Chiu WA, Rusyn I (2020) Temporal and spatial analysis of per and polyfluoroalkyl substances in surface waters of Houston ship channel following a large-scale industrial fire incident. Environ Pollut 265, Part B:115009. https://doi.org/10.1016/j.envpol.2020.115009

Anderson MJ (2001) A new method for non-parametric multivariate analysis of variance. Austral Ecology 26(1):32–46. https://doi.org/10.1111/j.1442-9993.2001.01070.pp.x

Arar EJ, Collins GB (1997) Method 445.0 In vitro determination of chlorophyll *a* and pheophytin a in marine and freshwater algae by fluorescence. U.S. Environmental Protection Agency, Washington, DC

Armstrong FAJ, Stearns CR, Strickland JDH (1967) The measurement of upwelling and subsequent biological processes by means of the Technicon Autoanalyzer and associated equipment. Deep-Sea Res 14(3):381–389. https://doi.org/10.1016/0011-7471(67)90082-4

Bernhardt H, Wilhelms A (1967) The continuous determination of low level iron, soluble phosphate and total phosphate with the AutoAnalyzer. Technicon Symposium

Bianchi TS, Osburn C, Shields MR, Yvon-Lewis S, Young J, Guo L, Zhou Z (2014) Deepwater horizon oil in Gulf of Mexico waters after 2 years: Transformation into the dissolved organic matter pool. Environ Sci Technol 48:9288–9297. https://doi.org/10.1021/es501547b

Blough NV, Zafiriou OC, Bonilla J (1993) Optical absorption spectra of waters from the Orinoco river outflow: terrestrial input of colored organic matter to the Caribbean. J Geophys Res 98:2271–2278

Brown MM, Mulligan RP, Miller RL (2014) Modeling the transport of freshwater and dissolved organic carbon in the Neuse River Estuary, NC, USA following Hurricane Irene (2011). Estuar Coast Shelf Sci 139:148–158. https://doi.org/10.1016/j.ecss.2014.01.005

Bugica K, Sterba-Boatwright B, Wetz MS (2020) Water quality trends in Texas estuaries. Mar Pollut Bull 152:110903. https://doi.org/10.1016/j.marpolbul.2020.110903

Cârstea EM, Ghervase L, Pavelescu G, Savastru D (2009) Assessment of the anthropogenic impact on water systems by fluorescence spectroscopy. Environ Eng Manag J 8(6):1321–1326

Catalá TS, Mladenov N, Echevarría F, Reche I (2013) Estuarine, coastal and shelf science positive trends between salinity and chromophoric and fluorescent dissolved organic matter in a seasonally inverse estuary. Estuar Coast Shelf Sci 133:206–216. https://doi.org/10.1016/j.ecss.2013.08.030

Catalá TS, Reche I, Fuentes-Lema A, Alvarez M, Romera-Castillo C, Nieto-Cid M, Ortega-Retuerta E, Calvo E, Marrasé C, Stedmon CA, Álvarez-Salgado XA (2015) Turnover time of fluorescent dissolved organic matter in the dark global ocean. Nat Commun 6:5986

Coble PG (1996) Characterization of marine and terrestrial DOM in seawater using excitation-emission matrix spectroscopy. Mar Chem 51(4) Elsevier BV:325–346. https://doi.org/10.1016/0304-4203(95)00062-3

Coble PG (2007) Marine optical biogeochemistry: the chemistry of ocean color. Chem Rev 107(2):402–418. https://doi.org/10.1021/cr050350+

D'Sa EJ, Joshi I, Liu B (2018) Galveston Bay and coastal ocean optical-geochemical response to Hurricane Harvey from VIIRS ocean color. Geophys Res Lett 45(19):10,579–10,589. https://doi.org/10.1029/2018GL079954

Du J, Kyeong P, Dellapenna TM, Clay JM (2019) Dramatic hydrodynamic and sedimentary responses in Galveston Bay and adjacent inner shelf to Hurricane Harvey. Sci Total Environ 653:554–564

Gabor RS, Baker A, Mcknight DM, Miller MP (2014) Fluorescence indices and their interpretation. In: Coble PG et al (eds) Aquatic Organic Matter Fluorescence, edited by. Cambridge Univ. Press, Cambridge, pp 202–228

Galveston Bay Estuary Program (2002) The state of the bay. A characterization of the Galveston bay ecosystem. In: Lester J, Gonzalez LA, Sage T, Gallaway A, 2nd Edn. http://hdl.handle.net/1969.3/26314

Gold AC, Thompson SP, Magel CL, Piehler MF (2020) Urbanization alters coastal plain stream carbon export and dissolved oxygen dynamics. Sci Total Environ 747:141132. https://doi.org/10.1016/j.scitotenv.2020.141132

Harwood JE, Kuhn AL (1970) A colorimetric method for ammonia in natural waters. Water Res 4:805–811. https://doi.org/10.1016/0043-1354(70)90037-0

Helms JR, Stubbins A, Ritchie JD, Minor EC, Kieber EJ, Mopper K (2008) Absorption spectral slopes and slope ratios as indicators of molecular weight, source, and photobleaching of chromophoric dissolved organic matter. Limnol Oceanogr 53(3):955–969

Hudson N, Baker A, Reynolds D (2007) Fluorescence analysis of dissolved organic matter in natural, waste and polluted waters—a review. River Res Appl 23:631–649. https://doi.org/10.1002/rra.1005

Huguet A, Vacher L, Relexans S, Saubusse S, Froidefond JM, Parlanti E (2009) Properties of fluorescent dissolved organic matter in the Gironde Estuary. Org Geochem 40(6):706–719. https://doi.org/10.1016/j.orggeochem.2009.03.002

Kida M, Fujitake N, Suchewaboripont V, Poungparn S, Tomotsune M, Kondo M, Ohtsuka T (2018) Contribution of humic substances to dissolved organic matter optical properties and iron mobilization. Aquat Sci 80(3):0. https://doi.org/10.1007/s00027-018-0578-z

Kothawala DN, Murphy KR, Stedmon CA, Weyhenmeyer GA, Tranvik LJ (2013) Inner filter correction of dissolved organic matter fluorescence. Limnol Oceanogr Methods 11(12) Wiley:616–630. https://doi.org/10.4319/lom.2013.11.616

Kowalczuk P, Cooper WJ, Whitehead RF, Durako MJ, Sheldon W (2003) Characterization of CDOM in an organic-rich river and surrounding coastal ocean in the South Atlantic Bight. Aquat Sci 65:384–401

Kulkarni HV, Mladenov N, Datta S, Chatterjee D (2018) Influence of monsoonal recharge on arsenic and dissolved organic matter in the Holocene and Pleistocene aquifers of the Bengal Basin. Sci Total Environ 637:588–599

Lawaetz AJ, Stedmon CA (2009) Fluorescence intensity calibration using the Raman scatter peak of water. Appl Spectrosc 63(8) SAGE Publications:936–940. https://doi.org/10.1366/000370209788964548

Legendre P, Gallagher ED (2001) Ecologically meaningful transformations for ordination of species data. Oecologia 129:271–280

Liu B, D'Sa EJ, Joshi ID (2019) Floodwater Impact on Galveston Bay phytoplankton taxonomy, pigment composition and photophysiological state following Hurricane Harvey from Field and Ocean Color (Sentinel 3A OLCI) Observations. Biogeosciences 16:1975–2001. https://doi.org/10.5194/bg-16-1975-2019

Loiselle SA, Bracchini L, Dattilo AM, Ricci M, Tognazzi A, Cózar A, Rossi C (2009) The optical characterization of chromophoric dissolved organic matter using wavelength distribution of absorption spectral slopes. Limnol Oceanogr 54(2):590–597. https://doi.org/10.4319/lo.2009.54.2.0590

Lu K, Liu Z (2019) Molecular level analysis reveals changes in chemical composition of dissolved organic matter from south Texas rivers after high flow events. Front Mar Sci 6. https://doi.org/10.3389/fmars.2019.00673

Massicotte P, Markager S (2016) Using a Gaussian decomposition approach to model absorption spectra of chromophoric dissolved organic matter. Mar Chem 180:24–32. https://doi.org/10.1016/j.marchem.2016.01.008

Massicotte P, Asmala E, Stedmon C, Markager S (2017) Global distribution of dissolved organic matter along the aquatic continuum: across rivers, lakes and oceans. Sci Total Environ 609(July):180–191. https://doi.org/10.1016/j.scitotenv.2017.07.076

McKnight DM, Boyer EW, Westerhoff PK, Doran PT, Kulbe T, Andersen DT (2001) Spectrofluorometric characterization of dissolved organic matter for indication of precursor organic material and aromaticity. Limnol Oceanogr 46(1):38–48. https://doi.org/10.4319/lo.2001.46.1.0038

Murphy KR, Stedmon CA, Graeber D, Bro R (2013) Fluorescence spectroscopy and multi-way techniques. PARAFAC. Anal Methods 5(23):6557. https://doi.org/10.1039/c3ay41160e

Murphy KR, Stedmon CA, Wenig P, Bro R (2014) OpenFluor – an online spectral library of auto-fluorescence by organic compounds in the environment. Anal Methods 6:658–661

Ohno T (2002) Fluorescence inner-filtering correction for determining the humification index of dissolved organic matter. Environ Sci Technol 36(4):742–746. https://doi.org/10.1021/es0155276

R Core Team (2018) R: A language and environment for statistical computing. Vienna, Austria. https://www.R-project.org

Schlitzer R (2020) Ocean Data View. odv.awi.de

Shiller AM, Shim M, Guo L, Bianchi TS, Smith RW (2012) Hurricane Katrina impact on water quality in the East Pearl River , Mississippi. J Hydrol 414–415:388–392. https://doi.org/10.1016/j.jhydrol.2011.11.010

Shutova Y, Baker A, Bridgeman J, Henderson HK (2014) Spectroscopic characterisation of dissolved organic matter changes in drinking water treatment: from PARAFAC analysis to online monitoring wavelengths. Water Res 54:159–169

Šmilauer P, Lepš (2014) Multivariate analysis of ecological data using CANOCO 5, 2nd edn. Cambridge University Press

Stedmon CA, Bro R (2008) Characterizing dissolved organic matter fluorescence with parallel factor analysis: a tutorial. Limnol Oceanogr Methods 6:572–579

Stedmon CA, Markager S, Kaas H (2000) Optical properties and signatures of chromophoric dissolved organic matter (cdom) in Danish coastal waters. Estuar Coast Shelf Sci 51:267–278

Stedmon C, Markager S, Bro R (2003) Tracing dissolved organic matter in aquatic environments using a new approach to fluorescence spectroscopy. Mar Chem 82:239–254

Steichen JL, Labonte JM, Windham R, Hala D, Kaiser K, Setta S, Faulkner PC, Bacosa H, Yan G, Kamalanathn M, Quigg A (2020) Microbial, physical, and chemical changes in Galveston bay following an extreme flooding event, Hurricane Harvey. Front Mar Sci 7. https://doi.org/10.3389/fmars.2020.00186

Stier AC, Geange SW, Hanson KM, Bolker BM (2013) Predator density and timing of arrival affect reef fish community assembly. Ecology 94:1057–1068

Strickland JDH, Parsons TR (1972) A practical handbook of seawater analysis. Bulletin 167, Journal of the Fisheries Research Board of Canada, Ottawa, Canada

Tanaka K, Kuma K, Hamasaki K, Yamashita Y (2014) Accumulation of humic-like fluorescent dissolved organic matter in the Japan Sea. Sci Rep 4:5292

ter Brak CJF, Šmilauer P (2012) CANOCO reference manual and user's guide: software for ordination (version 5.0). Microcomputer Power, Ithaca, p 496

Thyng KM, Hetland RD, Socolofsky SA, Fernando N, Turner EL, Schoenbaechler C (2020) Hurricane Harvey caused unprecedented freshwater inflow to Galveston Bay. Estuar Coasts 43:1836–1852. https://doi.org/10.1007/s12237-020-00800-6

Tzortziou M, Zeri C, Dimitriou E, Ding Y, Jaff R, Anagnostou E, Pitta E, Mentzafou A (2015) Colored dissolved organic matter dynamics and anthropogenic influences in a major transboundary river and its coastal wetland. Limnol Oceanogr 60(4):1222–1240. https://doi.org/10.1002/lno.10092

UNESCO/ICES/SCOR/IAPSO (1980) Joint panel on oceanographic tables and standards. Sidney, B. C., Canada

Valle-Levison A, Olabarrieta M, Heilman L (2020) Compound flooding in Houston-Galveston Bay during Hurricane Harvey. Sci Total Environ 747:141272. https://doi.org/10.1016/j.scitotenv.2020.141272

van Oldenborgh GJ, van der Wiel K, Sebastian A, Singh R, Arrighi J, Otto F, Haustein K, Li S, Vecchi G, Cullen H (2018) Corrigendum: attribution of extreme rainfall from Hurricane Harvey, August 2017. Environ Res Lett 12:124009. https://doi.org/10.1088/1748-9326/aaa343

Warnken KW, Santschi PH (2004) Biogeochemical behavior of organic carbon in the Trinity River downstream of a large reservoir lake in Texas, USA. Sci Total Environ 329:131–144

Yamashita Y, Maie N, Briceño H, Jaffe R (2010) Optical characterization of dissolved organic matter in tropical rivers of the Guayana Shield, Venezuela. J Geophys Res 115:G00F10

Yan G, Labonte JM, Quigg A, Kaiser K (2020) Hurricanes accelerate dissolved organic carbon cycling in coastal ecosystems. Front Mar Sci 7. https://doi.org/10.3389/fmars.2020.00248

Zheng Q, Chen Q, Cai R, He C, Guo W, Wang Y, Shi Q, Chen C, Jiao N (2019) Molecular characteristics of microbially mediated transformations of Synechococcus-derived dissolved organic matter as revealed by incubation experiments. Environ Microbiol 21:2533–2543. https://doi.org/10.1111/1462-2920.14646